Appendix

Appendix Table 1. Patient Characteristics and Timelines. *Dates of comparison studies or treatment are relative to the HP pyruvate studies, with negative numbers meaning prior to and positive numbers meaning following.

Patient	1	2	3	4
Mean Age = 61 Range = (47-73) 2 F and 2 M	47M	64F	73M	60F
Histopathological assessment of resected specimen	Anaplastic oligodendroglioma grade III Components of anaplastic oligodendroglioma are seen in a background of lower grade disease	Recurrent/residual high grade glioma with treatment effect – 60 % viable tumor and 40% necrosis	Metastatic malignant melanoma	Synchronous cerebellar metastasis resection : Metastatic high grade serous carcinoma (ovarian)
Prior Treatment	Bevacizumab and Temozolamide (50 mg/m^2)	Gross Total Resection, Radiation (60 Gy) and Nivolumab	None	Multiple systemic chemotherapy courses including Paclitaxel, Carboplatin, Cisplatin, Doxorubicin, Topotecan, and Bevacizumab
Days* to brain MR with DCE perfusion	2	0	-1	0
Days to ^{18}FDG PET/CT	244	NA	31	NA
Days to Start of Treatment	-172	-210	NA	-685
Days to end of Treatment	-111	-20	NA	-160
Days to Radiation Completion	NA	-151	NA	NA
Days to Resection	4	2	3	NA

Appendix Table 2. Quality Control Data for each dissolution.

Patient	Injected Dose (mL)	Pyruvate conc. (mM)	pH	EPA conc. (uM)	Temp (°C)	Polarization (%)	Polarization time (hr:min)	Time to injection (s)	Adverse Event
1	45.0	243.0	7.6	1.1	36.6	38.6	3:17	73	No
2 #1	23.0	240.0	7.8	1.1	35.4	49.0	2:40	79	No
2 #2	23.0	228.0	7.8	0.5	34.5	29.8	4:48	76	No
3	40.0	240.0	7.5	0.5	33.8	28.6	3:47	70	No
4	27.0	255.0	7.6	1.8	34.4	35.3	1:47	77	No

Dynamic Modeling and fitting of k_{PL}

Whole-brain metabolic dynamics were considered using a simplified two-compartment model with unidirectional flux from intravascular pyruvate (V) to extracellular pyruvate (P) and lactate (L), Appendix Figure 1. This model captures the essential details of the dynamics consistent with an in-vitro study (1), and consistent with our observation showing no significant hyperpolarized lactate signal in the superior sagittal sinus on the timescale of the experiment. Our formulation builds on previous work (2), in the model and fitting procedure, based on the derivation of a closed form solution, noting that optimized strategies (3), and more sophisticated models are certainly possible (4).

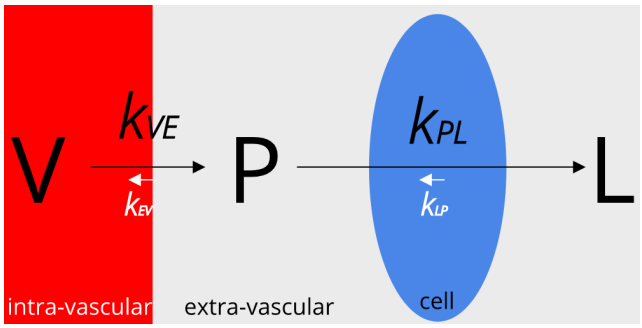

Appendix Figure 1. Simplified two-compartment model, considering only unidirectional forward flux from intravascular pyruvate (V), to extravascular pyruvate (P) and lactate (L). The back-rate constants, k_{EV} and k_{LP}, are assumed negligible and set to zero to simplify the model.

First-order rate constant kinetics were simulated, where the rate of change in a variable in unit volume was proportional to its concentration. The observed signal amplitude is then scaled by expected literature values for volume fractions for the intra-vascular (V_P = 0.07) and extravascular (V_E = 0.10) compartments during the fitting procedure (5). The vascular compartment is assumed to dominate the pyruvate signal, and used to derive the expected gamma-variate vascular input function (***V***) (see below). Flip angle (α) correction was averaged over the number of phase encodes (***PEs***) and repetition time (***TR***).

$$M = \begin{bmatrix} -k_{PL} - R_{1,P} + \frac{\log(\cos\alpha)PEs}{TR} & 0 & k_{VE} \\ k_{PL} & -R_{1,L} + \frac{\log(\cos\alpha)PEs}{TR} & 0 \\ 0 & 0 & 0 \end{bmatrix}$$

$$\begin{pmatrix} P(t) \\ L(t) \\ V(t) \end{pmatrix} \approx \exp(Md\tau) \begin{pmatrix} P(t-d\tau) \\ L(t-d\tau) \\ V(t-d\tau) \end{pmatrix} + \begin{pmatrix} 0 \\ 0 \\ V(t) - V(t-d\tau) \end{pmatrix}$$

The stationary approximation of the vascular input function improves as the recursion is equated to the integral ($d\tau \rightarrow 0$), the expression for which below can be further simplified using the Laplace Transform:

$$\begin{pmatrix} P(t) \\ L(t) \\ V(t) \end{pmatrix} = \int_0^t \exp(M\tau) \begin{pmatrix} P(0) \\ L(0) \\ V'(t-\tau) + V(0) \end{pmatrix}$$

For the purposes of simulating discretely sampled dynamics, the observed pyruvate and lactate time courses were interpolated 10-fold to approximate our assumptions of a stationary vascular input function over a single time-step. Constrained optimization was performed using the build-in MATLAB *fmincon* function. The flip angle was constrained to 25% of its calibrated value (7.5 – 12.5 °) with a known amplitude schedule for each TR. The pyruvate T1 was constrained to 50 s. The lactate T1 was constrained to 20-25 s. The kinetic rates k_{PL} and k_{VE} were essentially unconstrained, range = (0, 10^3 s^{-1}). The intra-vascular fraction was constrained (V_P range = 0 – 0.1); the extravascular volume fraction was set V_E = 0.10. The energy function used is an L2-norm, where the pyruvate profile was constrained to be the sum of the input function and extravascular pyruvate, with scaling normalizing the pyruvate and lactate amplitudes, and bias ($\gamma = 10^2$) toward the lactate profile which is more sensitive to K_{PL}. The reported errors are standard deviations obtained by the jack-knife procedure applied to the time-course (i.e. omitting a time point from the energy function).

$$E = \left(\frac{1}{\|P_{obs}\|} (V_E P_{fit} + V_P V_{fit} - P_{obs})^2 + \frac{\gamma}{\|L_{obs}\|} (V_E L_{fit} - L_{obs})^2 \right)^{1/2}$$

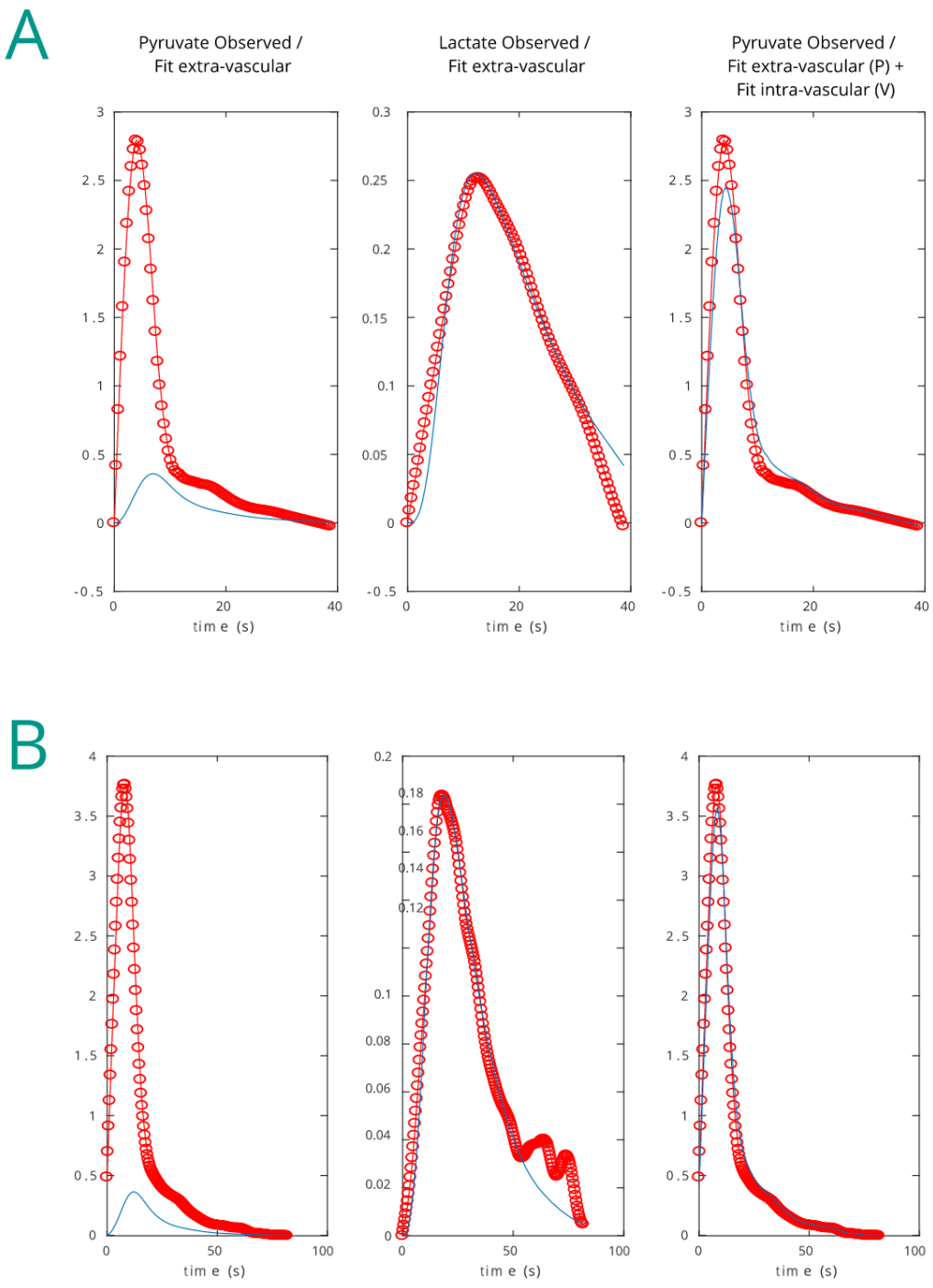

Appendix Figure 2. Kinetic model fit for Patient 4 (A) and Patient 1 (B). Observed data (red circles) is 10-fold interpolated from the acquired 4.3 s time resolution. Fitted data is plotted as a blue line. (Left) Total observed pyruvate signal and fitted extra-vascular pyruvate. (Middle) Total observed lactate and fitted extravascular lactate. (Right) Total observed pyruvate and the sum of fitted extra-vascular and intravascular pyruvate. The discrepancy can be attributed to a vascular component which is not available for transport to the extravascular space.

Appendix Table 3. Summary of whole brain fitted kinetic parameters in individual patients. Note that for patient 3 the tumor component dominates lactate production. For patient 4 (highest relative SNR) the imaging slice is localized on the cortex at the convexity. Tabulated values are means and jack-knife standard deviations.

Patient	1	2	3	4
k_{PL} (s^{-1})	0.08 ± 0.001	0.17 ± 0.02	0.1 ± 0.01	0.16 ± 0.01
k_{VE} (s^{-1})	0.003 ± 0.001	0.003 ± 0.001	0.001 ± 0.01	0.005 ± 0.001
Vp	0.09 ± 0.001	0.09 ± 0.002	0.09 ± 0.001	0.08 ± 0.005

Appendix References

1. Harrison C, Yang C, Jindal A, DeBerardinis RJ, Hooshyar MA, Merritt M, et al. Comparison of Kinetic Models for Analysis of Pyruvate-to-Lactate Exchange by Hyperpolarized (13)C NMR. NMR in biomedicine. 2012;25(11):1286-94.
2. Bankson JA, Walker CM, Ramirez MS, Stefan W, Fuentes D, Merritt ME, et al. Kinetic Modeling and Constrained Reconstruction of Hyperpolarized [1-13C]-Pyruvate Offers Improved Metabolic Imaging of Tumors. Cancer Research. 2015;75(22):4708-17.
3. Maidens J, Gordon JW, Arcak M, Larson PEZ. Optimizing flip angles for metabolic rate estimation in hyperpolarized carbon-13 MRI. IEEE transactions on medical imaging. 2016;35(11):2403-12.
4. Sourbron SP, Buckley DL. Tracer kinetic modelling in MRI: estimating perfusion and capillary permeability. Physics in medicine and biology. 2012;57(2):R1-33.
5. Marjanska M, Iltis I, Shestov AA, Deelchand DK, Nelson C, Ugurbil K, et al. In vivo 13C spectroscopy in the rat brain using hyperpolarized [1-(13)C]pyruvate and [2-(13)C]pyruvate. J Magn Reson. 2010;206(2):210-8.